Am J Physiol Heart Circ Physiol
280: H222–H236, 2001.

Effect of erythrocyte aggregation on velocity profiles in venules

JEFFREY J. BISHOP,[1] PATRICIA R. NANCE,[1] ALEKSANDER S. POPEL,[2]
MARCOS INTAGLIETTA,[1] AND PAUL C. JOHNSON[1]
[1]*Department of Bioengineering University of California, San Diego, La Jolla, California 92093; and*
[2]*Department of Biomedical Engineering, Johns Hopkins University, Baltimore, Maryland 21205*

Received 1 May 2000; accepted in final form 13 July 2000

Bishop, Jeffrey J., Patricia R. Nance, Aleksander S. Popel, Marcos Intaglietta, and Paul C. Johnson. Effect of erythrocyte aggregation on velocity profiles in venules. *Am J Physiol Heart Circ Physiol* 280: H222–H236, 2001.—A recent whole organ study in cat skeletal muscle showed that the increase in venous resistance seen at reduced arterial pressures is nearly abolished when the muscle is perfused with a nonaggregating red blood cell suspension. To explore a possible underlying mechanism, we tested the hypothesis that red blood cell aggregation alters flow patterns in vivo and leads to blunted red blood cell velocity profiles at reduced shear rates. With the use of fluorescently labeled red blood cells in tracer quantities and a video system equipped with a gated image intensifier, we obtained velocity profiles in venous microvessels (45–75 μm) of rat spinotrapezius muscle at centerline velocities between 0.3 and 14 mm/s (pseudoshear rates 3–120 s^{-1}) under normal (nonaggregating) conditions and after induction of red blood cell aggregation with Dextran 500. Profiles are nearly parabolic (Poiseuille flow) over this flow rate range in the absence of aggregation. When aggregation is present, profiles are parabolic at high shear rates and become significantly blunted at pseudoshear rates of 40 s^{-1} and below. These results indicate a possible mechanism for increased venous resistance at reduced flows.

venous resistance; blood constitutive equation; in vivo blood viscosity; in vivo fluorescence microscopy; wall shear stress

VENOUS VASCULAR RESISTANCE in skeletal muscle is highly dependent on blood flow, with resistance increasing as flow decreases (12, 25, 26, 29, 41). Previous rotational viscometric studies showed that the apparent viscosity of blood increases at low shear rates (9, 13, 14, 30) and that this increase is due primarily to red blood cell aggregation (13, 14). Because this effect occurs in the physiological range of shear rates in venous vessels, we hypothesized that red blood cell aggregation is an important determinant of venous resistance. Recent studies in our laboratory (12) on the lateral gastrocnemius muscle preparation of the cat have shown that the increased venous resistance at low flow rates is dependent on the presence of formed elements of the blood and is greatly reduced when a nonaggregating suspension of red blood cells is used as the perfusate. As a possible mechanism to explain this increased resistance, we hypothesized that red blood cell aggregates cause velocity profiles in venules to become more blunt than the parabolic shape expected for Poiseuille flow and, as a result, cause increased energy loss. There is evidence from in vitro studies in glass tubes (21, 35) that aggregation causes blunting of velocity profiles, but in vivo data are limited (36).

To test this hypothesis, we determined velocity profiles in skeletal muscle venules (45–75 μm in diameter) of the rat spinotrapezius muscle with the use of fluorescently labeled red blood cells. The rat provides an excellent model because rat red blood cells normally show negligible aggregation in rat plasma (4) but can be induced to aggregate using macromolecules such as high-molecular-weight dextran. This provided us with the ability to run our experimental protocol both with and without aggregation and compare the results. With the use of an intravital microscope equipped with a charge-coupled device camera and an externally gated image intensifier and videocassette recorder, we were able to record the position of labeled red blood cells during the gate open period of the image intensifier. With the use of image analysis, we then determined velocity profiles for normal (nonaggregating) and dextran-treated (aggregating) blood at control (up to 14 mm/s) and reduced flow rates.

MATERIALS AND METHODS

Animal preparation. Fourteen male Sprague-Dawley rats weighing between 250 and 400 g (mean 327.4 ± 41.5 g) were used for these investigations. Animal handling and care were provided following the procedures outlined in the *Guide for the Care and Use of Laboratory Animals* (NIH, National Research Council, 1996). The study was approved by the local animal subjects committee. Rats were anesthetized with an intraperitoneal injection of 50 mg/kg pentobarbital sodium (Abbott). Additional anesthetic was administered throughout the experiment as needed. The animal was placed on a heating pad to maintain body temperature during surgery. A trachea tube was inserted to assist breathing, the carotid artery was catheterized for blood withdrawals and pressure measurements, and the jugular vein was catheterized for

Address for reprint requests and other correspondence: P. C. Johnson, Dept. of Bioengineering, Univ. of California, San Diego, La Jolla, CA 92093-0412. (E-mail: pjohnson@bioeng.ucsd.edu).

The costs of publication of this article were defrayed in part by the payment of page charges. The article must therefore be hereby marked "*advertisement*" in accordance with 18 U.S.C. Section 1734 solely to indicate this fact.

administration of anesthetic, Dextran 500, FITC-dextran, or DiI-labeled red blood cells. All catheters were filled with a solution of heparinized saline (30 IU/ml) to prevent clotting.

An exteriorized rat spinotrapezius muscle preparation similar to that described previously (38) was used for these studies. The skin was opened to expose the spinotrapezius muscle. A drip of warm Plasma-Lyte A, adjusted to pH 7.4 (Baxter), was maintained throughout surgery to keep the muscle moist. Connective tissue was cleared from the surface of the muscle, and the muscle was separated from the surrounding tissue with the blood supply left intact. The animal was then placed on a Plexiglas platform with a raised area that enabled viewing of the muscle while maintaining normal blood flow. Size 4.0 sutures were attached to the outer edges of the muscle and used to secure the muscle to the platform. Moist gauze was placed around the edges of the muscle and covered with petroleum jelly, after which the muscle was suffused with Plasma-Lyte A and covered with a thin polyvinyl film (Saran Wrap, Dow Corning) while air bubbles were removed from the muscle surface. A temperature probe was placed beside the muscle, and temperature was maintained throughout the experiment by regulation of a heating element attached to the animal platform.

Microscope system. A schematic diagram of the experimental setup used for these investigations is shown in Fig. 1. An intravital microscope (Ortholux II, Leitz) equipped for both epi- and transillumination was used with Leitz ×25 (numerical aperture 0.6) and Olympus ×40 (numerical aperture 0.7) water immersion objectives and a Leitz UM20 (0.33) condenser lens. The image was projected onto an externally controlled gated image intensifier (GenIISys, Dage MTI) with a black and white video camera (CCD-72, Dage MTI) connected to a videocassette recorder (SVO-9500MD, Sony) and viewed on a monitor (SSM-121, Sony). This arrangement provided full-screen magnifications of the video image of ×750 (340 μm horizontal) and ×870 (300 μm horizontal) for the ×25 and ×40 objectives, respectively. Preliminary reports of this method have been given in abstract form (6, 7), and a similar setup has also been reported by Parthasarathi et al. (31). The muscle preparation was illuminated with a 100-W mercury arc lamp (model 1149, Walker Instruments, Scottsdale, AZ). A rotatable turret contained filters for viewing both DiI (XF101 VIVID, exciter: 525RDF45; dichroic: 557DRLP; emitter: 565EFLP; Omega Optical) and FITC (I2, exciter: BP 450–490; dichroic: RKP 510; emitter: LP515; Leitz) fluorescence emission under epi-illumination as well as an open position for viewing images under transillumination.

Hematocrit, aggregation, and pressure measurements. The hematocrit and degree of red blood cell aggregation were measured during the control period and after infusion of Dextran 500. Hematocrit was determined after centrifugation with a microhematocrit centrifuge (Readacrit, Clay Adams). The degree of red blood cell aggregation was assessed from triplicate measurements on a 0.35-ml blood sample with a photometric rheoscope (Myrenne Aggregometer, Myrenne,

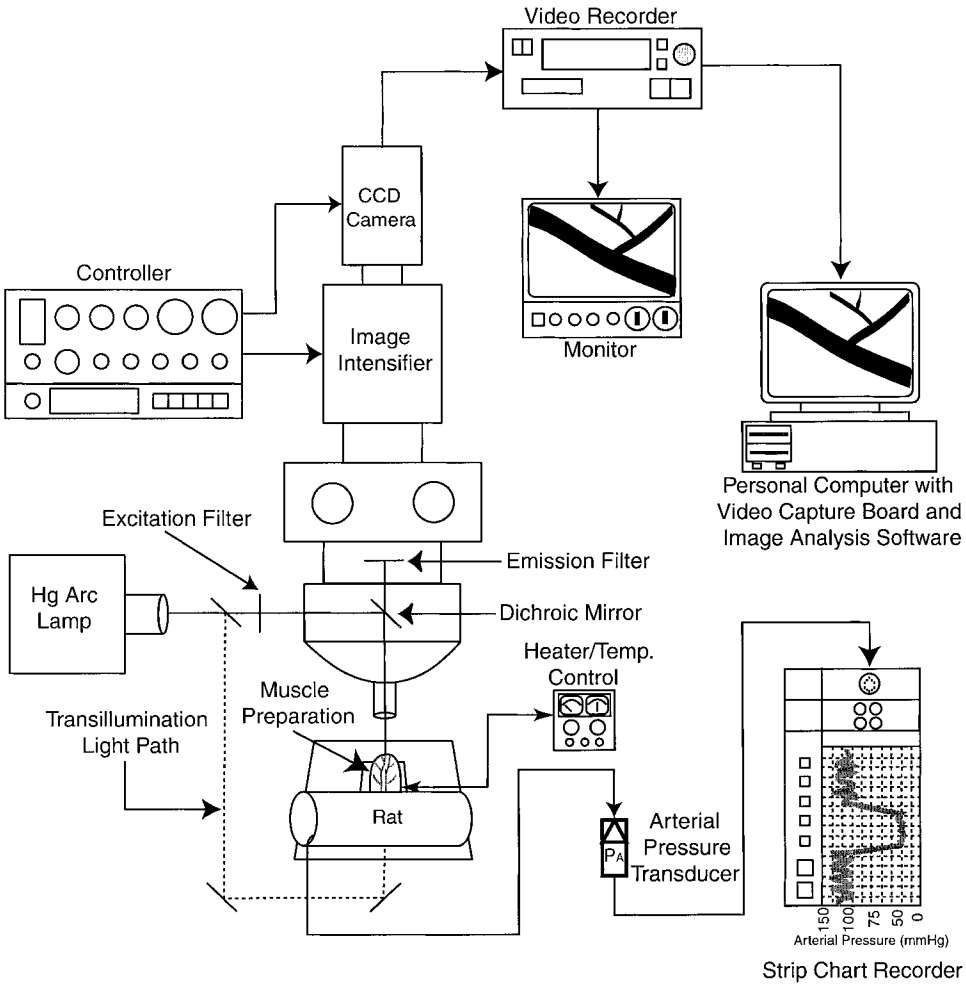

Fig. 1. Schematic diagram of the experimental setup, including an intravital microscope equipped for both trans- and epi-illumination. An externally controlled gated image intensifier allows for multiple images to be combined and recorded on a single video frame for determination of cell velocities up to 14 mm/s. A personal computer with video capture board allows the recorded image to be converted to digital format for image analysis. CCD, charge-coupled device.

Roetgen, Germany). The use of this technique as well as comparisons of this index of aggregation (M) with other methods and with different animal species has been described previously by Baskurt et al. (4, 5). The aggregation index (M) on the 10-s setting was used for these investigations. Erythrocyte sedimentation rate (ESR) of the same blood sample was also measured in triplicate in microhematocrit tubes allowed to stand for 1 h. The carotid artery catheter was attached to a pressure transducer (TNF-R, Viggo Spectramed) connected to a strip chart recorder (Brush 2600, Gould) for determination of arterial pressure. Pressure was recorded continuously throughout the experimental protocol and manually transferred into a microcomputer (300-MHz Pentium II, Micron) from the strip chart recordings for later analysis.

To compare our data with those of other investigators, we also measured the index of aggregation for samples of hamster blood provided to us by Dr. Amy Tsai of our laboratory.

Fluorescent labeling. Red blood cells to be used as tracers were fluorescently labeled with the carbocyanine dye 1,1′-dioctadecyl-3,3,3′,3′-tetramethylindocarbocyanine perchlorate ($DiIC_{12}$ (3); Molecular Probes) according to the method described by Unthank et al. (42). As discussed in that paper, this dye has been used to label a number of different cell types, and no alteration in any physical property of the cell, such as flexibility, due to this labeling procedure has been noted. We examined labeled cells under transillumination both in vivo and on a microscope slide and observed apparently normal cell shape and presence in red blood cell aggregates. Briefly, ~1.0 ml of blood was collected into a heparinized centrifuge tube (polypropylene, Fisher) from the carotid artery catheter. The red blood cells were separated from the whole blood by centrifugation (for 10 min) and aspiration of the plasma and buffy coat and then washed twice in a physiological saline solution (Hanks' balanced salt solution 1×; Cellgro). In four heparinized tubes, 0.15 ml of DiI was dissolved in 10 ml of Hanks' balanced salt solution solution, and one-fourth (~0.1 ml) of the packed red blood cells was added to the dye solution in each of the tubes. The cells were then incubated at room temperature in the dye solution for 30 min accompanied by mild mixing by hand rotation every 10 min. After the incubation period, we washed the red blood cells three times in the saline solution to remove unbound dye.

Experimental protocol. Initially, a 0.35-ml arterial blood sample was taken to determine control values of hematocrit and aggregation index. DiI-labeled cells were infused into the animal so as to obtain an in vivo concentration of ~1%. Next, a 1.0% solution of FITC ("Isomer 1," Molecular Probes) was infused into the bloodstream to achieve a concentration of 6 mg/kg body wt at the beginning of the experiment. This fluorescent label binds to albumin in the blood plasma and enables clear determination of the venular internal diameter.

A 45- to 75-μm diameter skeletal muscle venule with at least one side branch in the field of view was selected for study on the basis of the criteria of stable flow as well as clear focus and contrast of the image. The microscope was focused on the equatorial plane of the venule, and the video camera was oriented with the venule longitudinal axis diagonally on the video screen to maximize the distance available to follow red blood cell movement. A video image of the vessel was recorded under control conditions for successive 2-min periods with transillumination, excitation of the FITC dye, and excitation of DiI. Blood was then removed from the rat via the carotid artery into a heparinized syringe until arterial pressure was ~50 mmHg, and blood flow was allowed to stabilize. An average of 5.9 ± 1.8 ml of blood were withdrawn at a rate of ~2.5 ml/min to achieve this condition. The video image was again recorded at this reduced flow state under each of the three illumination conditions for ~2 min each, after which blood was reinfused into the animal over the course of 60–90 s. The arterial pressure was monitored until it returned to a steady-state value, and, in each case, these values were not significantly different from control values.

This protocol was then repeated ~20 min after addition of Dextran 500 (average molecular mass 460 kDa; Sigma) to induce red blood cell aggregation. Treatment groups before and after dextran infusion are hereafter denoted as normal and dextran groups. The dextran (200 mg/kg body wt) was dissolved in saline (6%) and infused in 50 mg/kg increments over the course of 2–3 min. Occasionally, a minor (<25 mmHg) drop in arterial pressure occurred during infusion, which typically recovered to the control value in <2 min. On the basis of a total blood volume of 5.5% (2), an average hematocrit of 40%, and an average body weight of 325 g, this represents a plasma dextran concentration of ~0.6%. Hematocrit and aggregation index values were determined 15 min after dextran infusion. Although dextran is reported to cause anaphylactic reaction in this species, there was no discernable adverse reaction (e.g., visible swelling of the limbs) to the dextran infusion in any of the rats used for these investigations.

With the use of fluorescently labeled red blood cells in tracer quantities, we were able to distinguish and follow single red blood cells flowing in the venules during conditions of normal and reduced arterial pressure. To obtain velocities at normal flow rates (1–14 mm/s for venules of this diameter), the repetition rate of the gated image intensifier was set to frequencies of 30–180 s^{-1}. This procedure produces multiple images of single red blood cells on one video frame when the frequency is greater than the video framing rate (30 s^{-1}).

Determination of red blood cell luminal position and velocity. Video tape recordings of images containing labeled red blood cells and labeled plasma were transferred to digital format for computer image analysis after completion of the experimental protocol. For this purpose, the videocassette recorder was connected to a video capture board (DC30 Plus, miroVIDEO) installed in a microcomputer (300-MHz Pentium II, Micron), as shown in Fig. 1. The video frames were then digitized with Abobe Premier 4.0 (Adobe), and the image files were transferred to a compact disk (CD-Writer Plus 7200e, Hewlett-Packard) for analysis and storage. Image magnification was determined from the recorded image of a stage micrometer under transillumination.

Figure 2, *A–C*, shows videomicrographs of a typical vessel studied under transillumination, DiI epi-illumination, and FITC epi-illumination, respectively. In Fig. 2*B*, a gate open period of 5 ms was used, creating the six images of each red blood cell seen on this video frame. From the digitized images, we used an image analysis software package (SigmaScan Pro 4.0, SPSS) to obtain x- and y-axis coordinate data at 5-ms intervals for individual red blood cells. All cells with distinct images were followed during a short time period (up to 30 s) to obtain information at all radial positions in the venule lumen. These coordinate data were imported into a spreadsheet (EXCEL, Microsoft) where the radial and longitudinal positions for each red blood cell during each gate open period were determined and recorded. With the use of the same image analysis and spreadsheet software programs, venular wall position was determined from the transillumination and FITC fluorescence images, and these data were combined to obtain a composite diagram, such as that shown in Fig. 3. For clarity, only a fraction of the total number of cells analyzed in this vessel are shown. Approximately 75

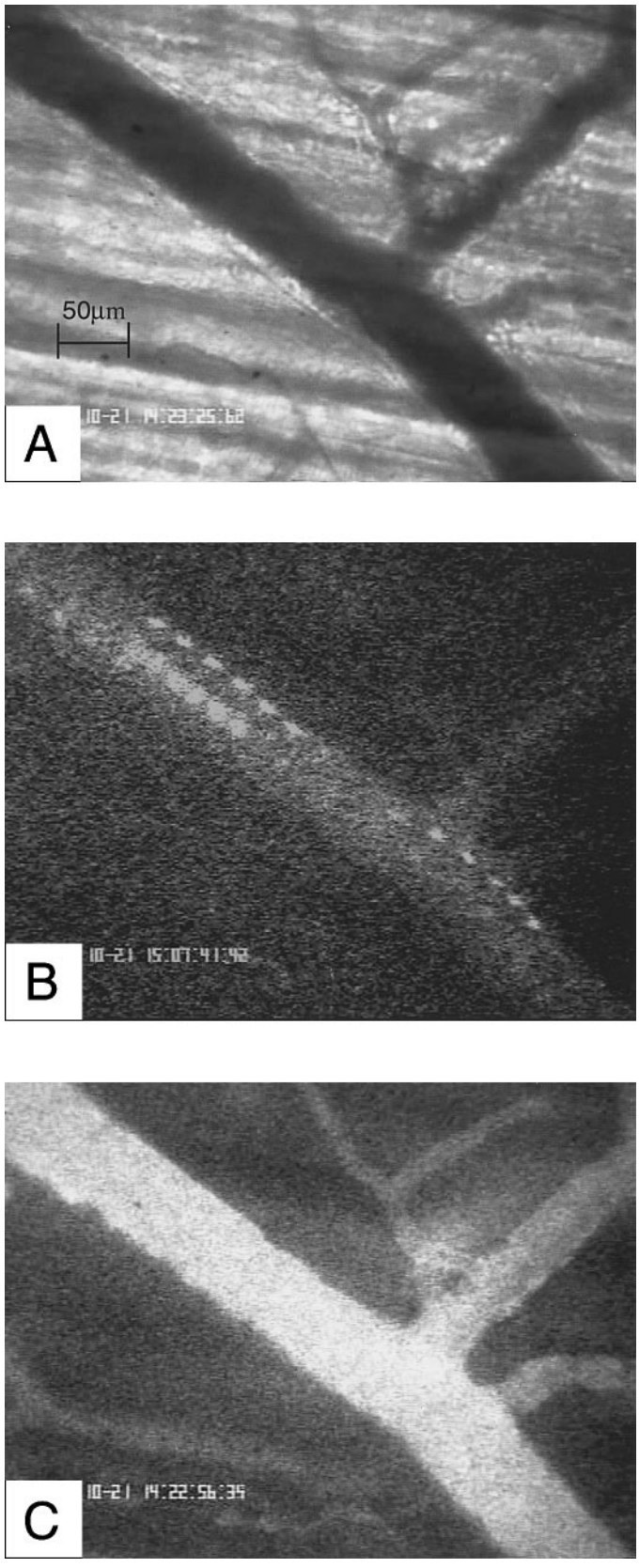

cells distributed across a 50-μm-diameter vessel were needed to obtain a statistically valid profile fit.

As also shown in Fig. 3, longitudinal sections ~100 μm in length were defined to obtain velocity profiles before venous junctions, directly after junctions, and further downstream from the junctions. Multiple determinations of velocity for each cell were obtained from the separation distance between successive images and the gate frequency. The velocity and radial position information for each cell were averaged within each longitudinal section and used to create a velocity profile.

An estimation of the error associated with marking the center of red blood cell images on the image analysis software was determined by a test of repeated measures on a group of 10 cells. The standard deviation of the distance between consecutive cell positions of 1.18 ± 0.32 μm for the fastest cells [maximum velocity (V_{max}) = 5.1 ± 1.0 mm/s; n = 10] was significantly greater ($P < 0.001$) than the standard deviation of 0.74 ± 0.12 μm for the slowest cells (V_{max} = 0.70 ± 0.17 mm/s; n = 10). Neither quantity was significantly different for any of the observers (n = 3) nor from the interobserver variability. The radial component of the error in marking cell position for the fastest cells (0.41 ± 0.19 μm) was not significantly different from the slowest cells (0.39 ± 0.18 μm). The greater variability in the fastest cells was likely due to elongation of the cell images during the gate open period.

Although venular diameters may vary slightly along the longitudinal axis due to lumen irregularities, we assumed a constant venular diameter within each section used for profile determination (longitudinal distance 100 μm) on the basis of the average wall position. The error associated with this approximation was determined by comparison of the actual with the average wall position at 0.8-μm intervals (n = 12). The standard deviation of this distance was 0.74 μm or ~1.5% of vessel diameter.

Statistical analysis. Both the *t*-test and the nonparametric Mann-Whitney rank sum test were used to determine differences in experimental and physiological parameters between normal and dextran-treated animals. Individual cell velocities and radial positions in each longitudinal section were averaged and plotted as means ± SE. Regression fits of individual profiles to the experimental data points were minimized using a linear least-squares algorithm designed for a standard software package (EXCEL, Microsoft). Regression lines for relationships between experimental parameters and red blood cell velocity or pseudoshear rate were determined by this same software package. On the basis of superior fit, curvilinear regression was used to describe the relationships between profile parameter data and pseudoshear rate or velocity for dextran-treated blood, whereas linear regression provided satisfactory fit for these relationships when describing normal blood. Correlation coefficients, 95% confidence intervals, and probability values for profile fits and regression lines were calculated with standard procedures described by Glantz (22). Differences in profile parameters between normal and dextran-treated rats were determined using both the paired *t*-test and the nonparametric Wilcoxon

Fig. 2. Videomicrographs of a sample venular network under transillumination (*A*), epi-illumination for DiI, (labeled red blood cells) (*B*) and epi-illumination for FITC (plasma) (*C*). Note in *B* a gate open period of 5 ms was used, creating 6 images of each cell on the single video frame. Images were converted from recorded videotape frames to digital format with the use of an image capture board attached to a microcomputer.

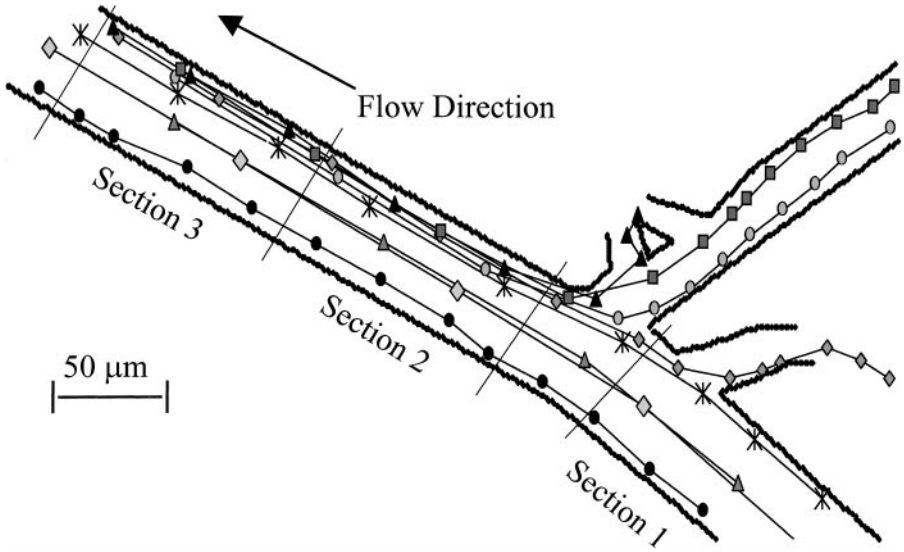

Fig. 3. Composite plot showing the position of labeled red blood cells at 5-ms intervals passing through the sample venular network shown in Fig. 2. Sections (100 μm) were selected before and after the bifurcation as shown for the determination of average velocity profiles at these locations.

signed rank test performed by a statistical software package (SigmaStat, Jandel). For all tests and regression fits, $P < 0.05$ was considered statistically significant.

RESULTS

Hematocrit, degree of aggregation, and arterial pressure. For normal rats, the hematocrit was 45.7 ± 5.4%, the index of aggregation (M) was 0.02 ± 0.1, the ESR was 0.5 ± 0.2 mm/h, and the arterial pressures were 123 ± 11 and 50 ± 14 mmHg during control and reduced flow situations, respectively. In dextran-treated rats, the hematocrit was 39.1 ± 6.7%, the index of aggregation was 11.7 ± 5.5, the ESR was 8.0 ± 0.4, and the arterial pressures were 132 ± 17 and 48 ± 14 mmHg for control and reduced flow situations, respectively. The mean hematocrit of the dextran-treated rats was significantly ($P < 0.001$) less than those of normal animals. There were no significant differences ($P > 0.05$) between arterial pressures of normal and dextran-treated animals during either the control or reduced flow situations.

For hamster blood samples ($n = 7$), the hematocrit was 49 ± 2%, and the index of aggregation was 0 ± 0.0.

Velocity profile determination. Velocity data were obtained on ~75 cells in each of the five vessels under control and reduced flow situations before and after induction of red blood cell aggregation. The gate frequency of the image intensifier was set so that ~25 images of each cell were obtained during transit of the cell across the video screen, totaling ~100,000 measurements of cell position for 4,000 cells. Figure 4 is an example of a velocity profile of normal (nonaggregating) blood at control arterial pressure obtained by plotting the position and velocity for all cells visible in *section 2* of the vessel shown in Fig. 3 while focused on the equatorial plane. While the parabolic nature of the leading edge of the profile can be observed, a number of velocity points fall substantially below this leading edge. Because the videomicrograph is a two-dimensional projection of a three-dimensional vessel, it was hypothesized that those velocity points falling well below the leading edge of the profile may have been from cells located above or below the equatorial plane and, therefore, would be out of focus to varying degrees.

Location of cells in equatorial plane of vessel. To test this assumption, a microscope slide prepared with labeled red blood cells was placed on the microscope stage, and videomicrographs were recorded as the sample was raised and lowered through the object plane of the microscope. After these images were digitized, a line intensity scan through a cell image was done to

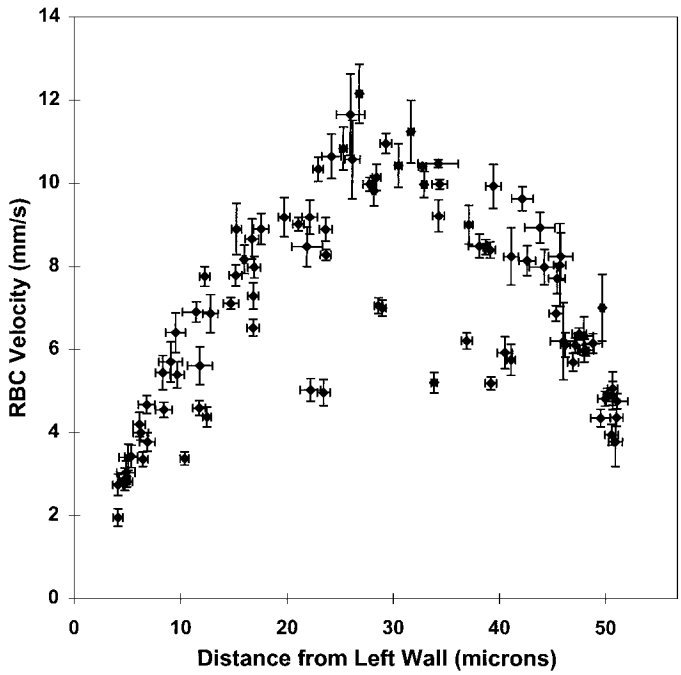

Fig. 4. Sample velocity profile for *section 2* (Fig. 3), including all labeled cells visible with the microscope focused on the equatorial plane of the vessel. Individual cell velocity and position values (means ± SE) within the section are plotted. RBC, red blood cells.

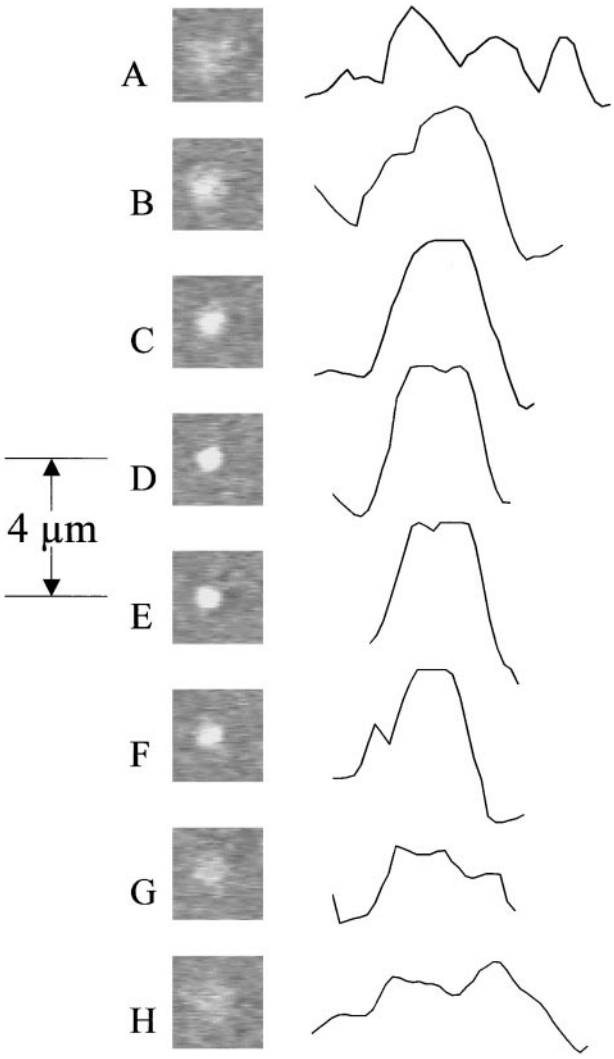

Fig. 5. In vitro red blood cell images and corresponding line intensity profiles with 4-μm vertical shifts of the microscope stage. The figure demonstrates that labeled cells in an 8-μm section encompassing the object plane present a narrow intense image (*C–E*), which can be distinguished from the wide image (*A* and *B* and *F–H*).

determine the cell intensity profile. Figure 5 shows the video images and corresponding line intensity plots for a single cell at 4-μm vertical intervals. This figure demonstrates that labeled cells in an 8-μm section encompassing the object plane present a narrow intense image (Fig. 5, *C–E*) that can be distinguished from the wide image (Fig. 5, *A* and *B* and *F–H*) for cells outside of this region. With the use of this method, it is possible to differentiate between cells in or out of a selected optical section on the basis of an objective criterion. This technique extends a previous study by Tangelder et al. (39), where the ability to localize fluorescent microspheres and blood cells within a thin optical section during flow was demonstrated.

To avoid the effect of cell movement during the gate open period, we measured only the width of the video image perpendicular to the flow direction. Cell width appeared to be independent of velocity because measured values were not significantly different ($P > 0.05$) during control and reduced flow situations. The relation between the width of the red blood cell image in vivo and its velocity can be seen in Fig. 6*A*, where cells from the velocity profile shown in Fig. 4 have been identified according to image width. When all cells with an image width >5.5 μm are removed, the profile shown in Fig. 6*B* is obtained. The fact that all points well below the leading edge of the profile are removed using this method is consistent with expectations.

Curve fitting of velocity profiles. After data were removed for cells out of the equatorial plane, a linear least-squares minimization algorithm developed for and solved by a standard software package (Excel, Microsoft) was used to fit profiles, like the one shown in Fig. 6B, to the equation

$$V(r) = V_{\max}\left(1 - \left|\frac{r}{R}\right|^{K}\right) \qquad (1)$$

where $V(r)$ is the velocity at radial position r, the vertical bars denote absolute value, $V_{\max}$ is the velocity in the center of the vessel, and R is the radius of the vessel. This equation satisfies the no-slip boundary condition at the vessel wall. The exponent K is a measure of the parabolic nature of the profile, with $K = 2$

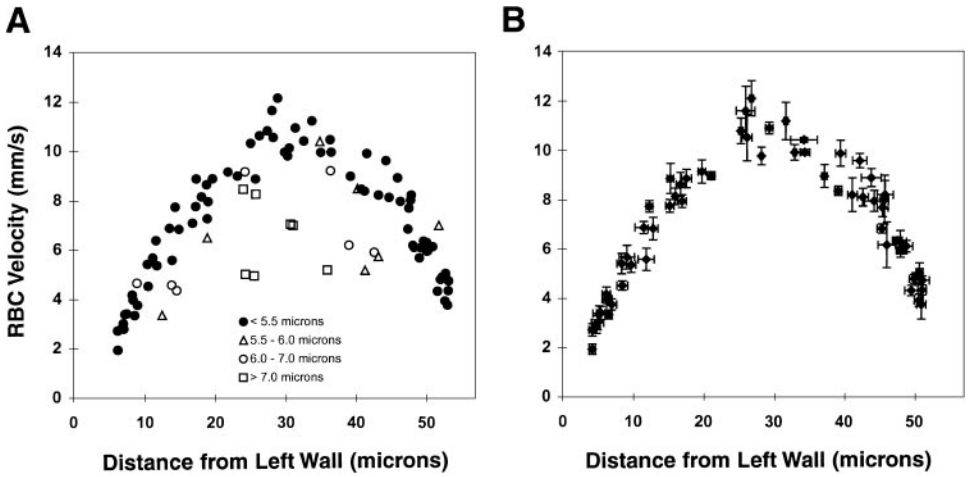

Fig. 6. Velocity profile for *section 2* (Figs. 3 and 4) with cells separated on the basis of image width (*A*) and after removal of all cells not in the equatorial plane (*B*) on the basis of the criteria of width > 5.5 μm.

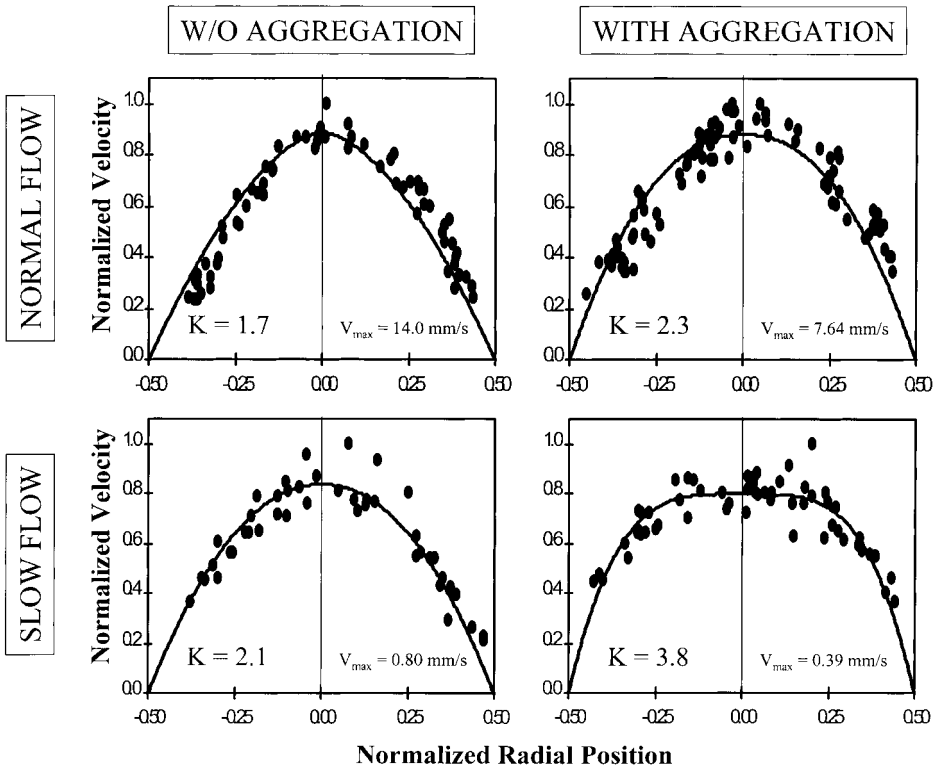

Fig. 7. Sample set of velocity profiles determined at normal and reduced flow-rates, before and after infusion of Dextran 500. V_{max}, maximum velocity; K, parameter denoting the parabolic nature of the profile. $P < 0.001$ for all regression lines.

for a parabola and $K > 2$ for a blunted profile. After error minimization, we calculated a correlation coefficient for each profile fit. This coefficient was then tested for statistical significance by conversion to a t-value, and, for each profile, the fit to the experimental data was statistically significant ($P < 0.001$).

Effect of aggregation on velocity profiles. Figure 7 shows the centerline velocity profiles obtained from *section 2* of the vessel described above (Fig. 3) under conditions of control and reduced flow for normal (nonaggregating) and dextran-treated (aggregating) blood. As expected, the nonaggregating profiles for both control and reduced flow rates are nearly parabolic ($K \approx 2$) in nature. When dextran was added to the circulating blood, red blood cell aggregation caused a slight blunting of the velocity profiles under control flow conditions and marked blunting at reduced flow.

Fifty-two velocity profiles similar to those shown in Figs. 6 and 7 were obtained in five venules of similar diameter (53.1 ± 7.8 μm) at locations before and after bifurcations with side branches of similar diameter (32.9 ± 8.3 μm) to that shown in Fig. 2. The exponent K for normal animals was 1.8 ± 0.4 at control arterial pressure and 2.1 ± 0.5 at reduced arterial pressure. For dextran-treated animals, K values were 2.2 ± 0.3 for control and 3.1 ± 0.6 for reduced arterial pressures, respectively. The bluntness parameter (K) for dextran-treated animals at reduced arterial pressure is significantly larger ($P < 0.01$) than for any of the other three conditions (normal animals at reduced arterial pressure, normal animals at control arterial pressure, and dextran-treated animals at control arterial pressure), which are not significantly ($P > 0.05$) different from one another. At control arterial pressures, centerline velocities in normal animals (V_{max} = 6.8 ± 3.6 mm/s) were significantly ($P < 0.05$) higher than those in dextran-treated animals (V_{max} = 5.3 ± 2.1 mm/s); at reduced arterial pressures, centerline velocities in normal animals (V_{max} = 0.49 ± 0.28 mm/s) were not significantly different ($P > 0.206$) than those in dextran-treated animals (V_{max} = 0.53 ± 0.19 mm/s).

The bluntness parameters (K) for each of these profiles versus V_{max} for normal and dextran-treated rats

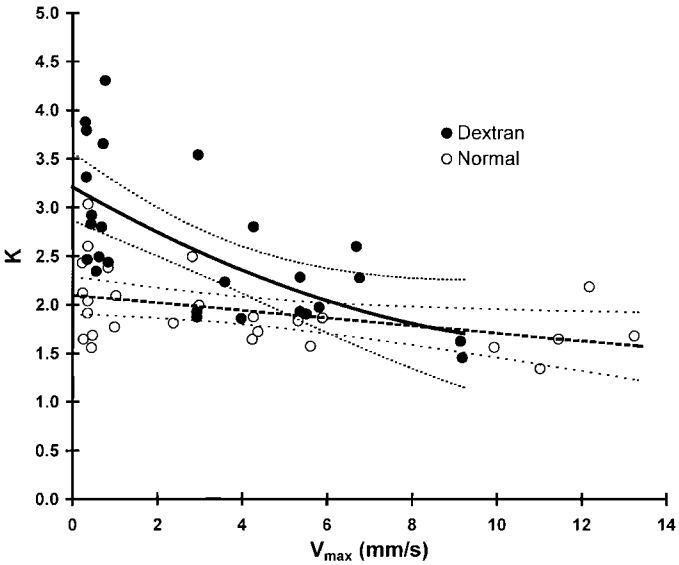

Fig. 8. Aggregation index parameter (K from *Eq. 1*) versus V_{max} for velocity profiles from normal and dextran-treated rats. $P < 0.02$ for both regression lines. Dotted lines show 95% confidence intervals.

are shown in Fig. 8. This graph shows the trends described for the profiles shown in Fig. 7, namely that the parabolic nature of nonaggregating blood is relatively unaffected by flow changes, whereas aggregating blood profiles become increasingly blunted as flow velocity decreases. Although from Fig. 8 there appears to be a trend for normal blood that might indicate a slight blunting effect at low flow rates, this slope was not significantly ($P > 0.05$) different from zero.

Determining the profile shape allows estimation of the mean velocity and volumetric flow rates by integration of the profiles. Assuming profile symmetry in three dimensions similar to that in two dimensions, the profiles were integrated, and the mean velocity (V_{mean}) was determined. The three-dimensional dimensionless velocity (3-D V_{mean}/V_{max}) is plotted in Fig. 9*A*. For a three-dimensional parabolic velocity profile, the mean velocity is one-half the V_{max}, and the normal (nonaggregating) data points are not significantly different from this value across the entire velocity range. However, in dextran-treated animals, V_{mean} reached 65% of the V_{max} in several venules at low flow rates.

The ratio of V_{mean} to V_{max} was also calculated by two-dimensional integration of the profiles and is shown in Fig. 9*B*. For a two-dimensional parabolic velocity profile, the V_{mean} is two-thirds the V_{max}, and the normal data points are not significantly different from this value across the velocity range. For dextran-treated animals, the two-dimensional V_{mean} reached 80% of the V_{max} in several venules at the lowest flow rates.

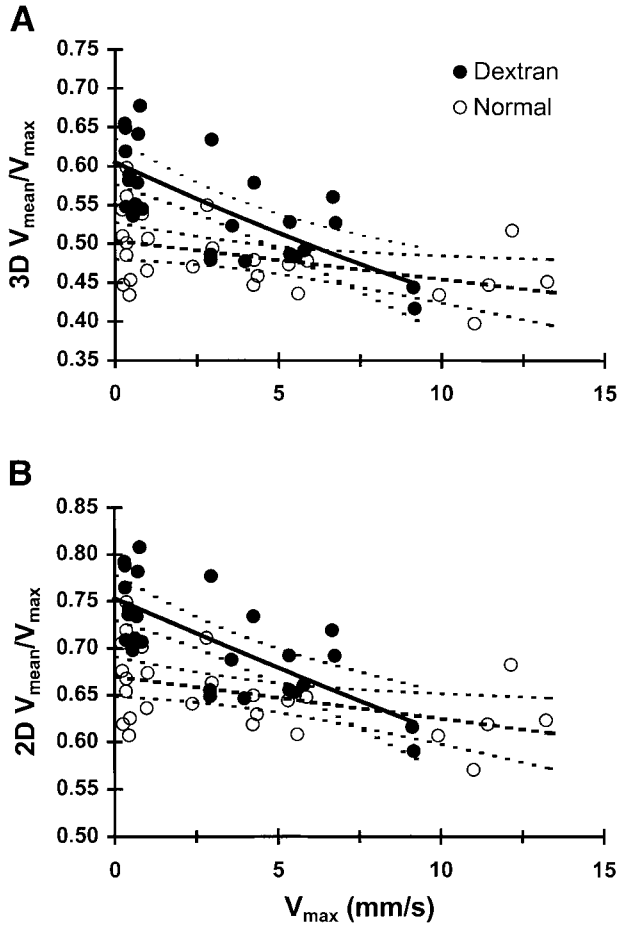

Fig. 9. Mean velocity (V_{mean})/V_{max} (from *Eq. 1*) ratio versus V_{max} (actual) for venules in normal and dextran-treated rats as determined by 3-dimensional (3D, *A*) and 2-dimensional (2D, *B*) numerical integration of the velocity profiles. $P < 0.01$ for all regression lines.

With the use of the value of V_{mean} obtained from three-dimensional integration of the profiles, the pseudoshear rate ($\bar{u} = V_{mean}/D$, in s^{-1}, where D is diameter) was determined for each section. Figure 10 shows the relationship between the parameter K from *Eq. 1* and the pseudoshear rate. This plot is substantially similar to the relationship between K and V_{max} (Fig. 8), but it emphasizes the fact that significant differences in profile shape between normal and dextran-treated blood can be detected at pseudoshear rates up to 40 s^{-1} and may be present at pseudoshear rates approaching 90 s^{-1}, where the intersection of the two regression lines occurs. A summary of the measured and analytically determined parameters for the profiles from each section is shown in Table 1. In this table, profiles have been grouped according to aggregation condition (normal or dextran-treated) and flow condition (control or reduced arterial pressure). A complete listing of the parameters for each individual profile is on file in the journal repository as Table A.[1]

Effect of aggregation on shear rate radial gradient. The radial variation of the local shear rate ($\dot{\gamma}$) can be calculated by differentiating the velocity distribution (*Eq. 1*) with respect to the radius, yielding the equation

$$\dot{\gamma} = \frac{dV}{dr} = \frac{K \cdot V_{max} \cdot r^{(K-1)}}{R^K} \qquad (2)$$

This relationship is shown graphically in Fig. 11 for dextran-treated and normal blood at $V_{max} = 0.2$ mm/s ($\bar{u} = 2\ s^{-1}$) and $V_{max} = 4.0$ mm/s ($\bar{u} = 40\ s^{-1}$) with the use of K values from Fig. 8. Because the profile with normal blood is parabolic, the shear rate increases linearly with the radius r and reaches a value eight times the pseudoshear rate at the vessel wall. In contrast, with dextran-treated blood, the shear rate in the central 60% of the vessel is below that for normal blood, whereas near the vessel wall it is much higher.

DISCUSSION

Principal finding. The purpose of this study was to test the hypothesis that red blood cell aggregates cause velocity profiles in venules to become more blunt than the parabolic shape expected for Poiseuille flow. Such an effect may lead to increased energy loss, as discussed in a later section. To this end, we made a detailed comparison of the shape of velocity profiles obtained in venous microvessels with both nonaggregating and aggregating blood. As shown in Figs. 8 and 10, profiles for nonaggregating blood are uniform and

[1]For Table A (Experimental Profile Data), order NAPS Document 05581 from NAPS % Microfiche Publications, PO Box 3513, Grand Central Station, New York, NY 10017.

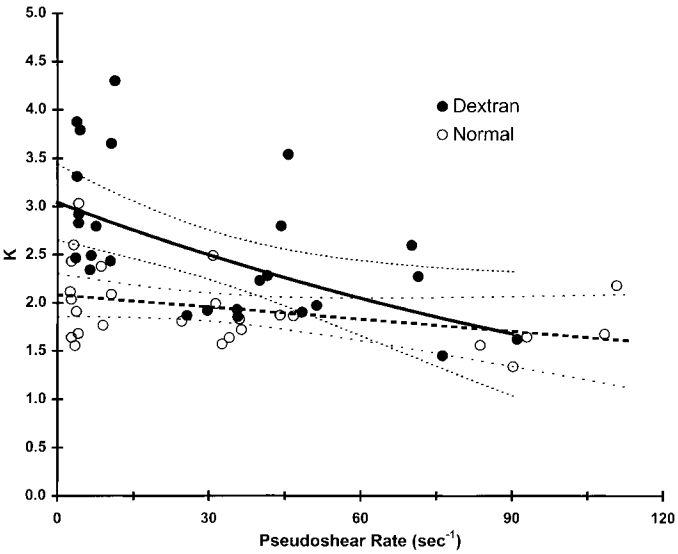

Fig. 10. Aggregation index parameter (K from *Eq. 1*) versus pseudoshear rate for velocity profiles from normal and dextran-treated rats. $P < 0.05$ for both regression lines. Dotted lines show 95% confidence intervals.

nearly parabolic over a large range of velocities and pseudoshear rates. In contrast, the shape of profiles for aggregating blood is shear rate dependent. At high flow rates, the parameter of profile shape (K) is similar for aggregating and nonaggregating bloods. The regression lines for the profile shape parameters of the two bloods diverge as pseudoshear rates are reduced below ~90 s^{-1}, and the blunting parameters become significantly different at 40 s^{-1} and below. These findings are consistent with the hypothesis that the flow properties of aggregating blood contribute to a rise in venous resistance of skeletal muscle at low flow rates. To our knowledge, this study is the first to examine the effect of changing velocity and red blood cell aggregability on velocity profiles in vivo.

Limitations of measurement. There are several sources of uncertainty in the method we used to determine red blood cell velocity. These errors are principally related to determining the center of each red blood cell image and the position of the venular wall. The errors involved in marking red blood cell positions (~1%), as discussed in MATERIALS AND METHODS, are independent and random. The error in determining the position of the vessel wall (~1.5%) was minimized (23) by combining information from both the transillumination and FITC epi-illumination images. Accounting for these sources of error, the estimated error of the profile bluntness parameter K is ±0.3. This error is less than the interexperimental scatter and does not significantly alter the present conclusions.

Comparison with velocity profiles from previous studies. A number of previous studies (1, 10, 11, 16, 19, 21, 31, 32, 35, 37, 39) have obtained velocity profiles in vivo or in vitro. In comparing profiles from different studies, careful attention must be paid to the technique of velocity measurement, the tube or vessel diameter, and erythrocyte aggregability. Velocity profiles have been determined by visualizing individual cells in the flow stream and storing the images with high-speed recording techniques or by monitoring photometric signals at two points and determining the time required for passage. The imaging technique has the advantage that the measurement can be limited to a narrow plane at the centerline (39, 40), whereas the photometric technique reports a weighted average throughout the flow stream (3, 32). As a result, imaging techniques can, in principle, determine the actual velocity profile, whereas photometric techniques would underestimate velocity except at the edge of the flowstream. Another consideration is the diameter of the tube or vessel because velocity profiles become more blunt as the tube or vessel diameter decreases (9, 10, 37) due to the increasing ratio of particle size to tube diameter. Additionally, because red blood cell aggregability varies

Table 1. *Summary of experimental profiles*

Vessel Section	P_A, mmHg	D, μm	V_{max}, actual, mm/s	V_{max} (From *Eq. 1*)	K (From *Eq. 1*)	V_{mean}/V_{max} (2D)	Q, nl/s	$\bar{u}$, s^{-1}
				Normal				
1	121.3 ± 11	51.8 ± 7.1	6.0 ± 3.9	0.86 ± 0.07	1.80 ± 0.11	0.64 ± 0.01	0.87 ± 0.65	71.3 ± 40.7
2	121.3 ± 11	57.6 ± 10.0	7.2 ± 4.3	0.86 ± 0.07	1.79 ± 0.40	0.63 ± 0.04	1.16 ± 0.64	79.5 ± 49.8
3	121.3 ± 11	55.5 ± 9.1	7.2 ± 4.1	0.85 ± 0.09	1.81 ± 0.32	0.64 ± 0.04	1.12 ± 0.67	83.1 ± 49.9
1	44 ± 16	47.9 ± 4.7	0.49 ± 0.33	0.84 ± 0.06	2.09 ± 0.64	0.66 ± 0.06	0.062 ± 0.047	6.5 ± 3.9
2	44 ± 16	54.9 ± 8.9	0.51 ± 0.34	0.86 ± 0.06	1.95 ± 0.27	0.66 ± 0.04	0.077 ± 0.040	6.4 ± 5.1
3	44 ± 16	53.4 ± 8.0	0.47 ± 0.26	0.86 ± 0.07	2.27 ± 0.41	0.69 ± 0.04	0.074 ± 0.042	6.1 ± 3.5
				Dextran				
1	126.7 ± 21	53.1 ± 4.2	4.5 ± 1.4	0.85 ± 0.06	1.99 ± 0.16	0.67 ± 0.02	0.67 ± 0.28	55.6 ± 15.5
2	126.7 ± 21	55.0 ± 10.5	5.6 ± 2.5	0.86 ± 0.05	1.89 ± 0.29	0.65 ± 0.04	0.88 ± 0.45	67.4 ± 31.1
3	126.7 ± 21	52.6 ± 10.6	5.7 ± 2.4	0.85 ± 0.07	2.57 ± 0.57	0.71 ± 0.06	0.87 ± 0.39	76.3 ± 31.3
1	46.2 ± 11	48.5 ± 4.3	0.51 ± 0.24	0.78 ± 0.11	2.64 ± 0.45	0.72 ± 0.03	0.064 ± 0.018	7.8 ± 4.2
2	46.2 ± 11	51.9 ± 7.4	0.54 ± 0.20	0.76 ± 0.11	3.38 ± 0.82	0.77 ± 0.05	0.086 ± 0.028	8.2 ± 3.9
3	46.2 ± 11	54.2 ± 10.4	0.53 ± 0.20	0.77 ± 0.08	3.29 ± 0.56	0.76 ± 0.03	0.082 ± 0.023	8.0 ± 3.9

All values reported as means ± SD. P_A, arterial pressure; D, diameter; V_{max}, maximum velocity; K, parameter measuring the parabolic nature of the profile; V_{mean}, mean velocity; 2D, 2-dimensional; Q, flow; $\bar{u}$, pseudoshear rate.

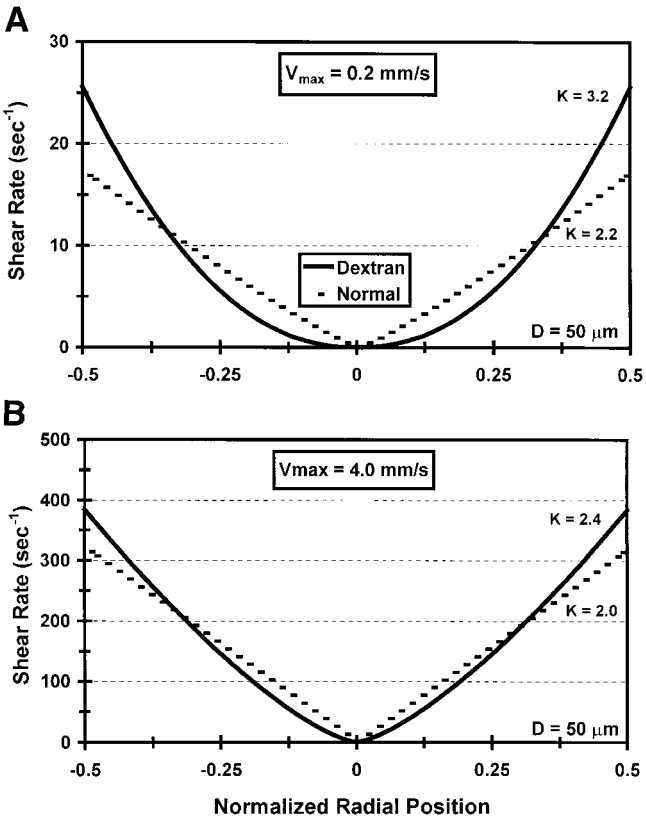

Fig. 11. Comparison of radial shear rate distribution for normal and dextran-treated blood in a 50-μm-diameter (D) venule at V_{max} = 0.2 mm/s (A) and V_{max} = 4.0 mm/s (B). Relationships are computed from *Eq. 2* using flow rate and profile blunting parameters from Fig. 8.

widely by species (4, 33, 43), the degree of blunting seen in the velocity profiles would also be species dependent. Table 2 shows how the normal and dextran-treated blood of the present study compares in aggregability (as measured by ESR or index of aggregation values) to blood from species used in previous studies.

The only other extensive studies on velocity profiles of aggregating blood are those done on human blood in vitro. Bugliarello and co-workers (10, 11) reported that velocity profiles of human blood in 40- or 70-μm-diameter glass tubes obtained with high-speed microcinematography were blunted at low flow rates (~50 s^{-1}) and became more parabolic with increased flow rate or greater tube diameter, although a quantitative description of this relationship was not given. Reinke et al. (35) found that velocity profiles of fluorescently labeled human red blood cells became increasingly blunted as pseudoshear rates in a 66-μm tube were decreased from 26.4 to 0.69 s^{-1}. Gaehtgens et al. (21) determined velocity profiles of human blood in 30- to 130-μm glass tubes for pseudoshear rates of 1–300 s^{-1} with the use of the dual-sensor method (44). Their profile bluntness parameter decreased as shear rate increased but was not parabolic even at the highest shear rates. The inverse trend between profile bluntness and shear rate seen in these studies agrees with the present findings for dextran-treated blood.

Previous in vivo studies of velocity profiles have used species (hamsters and rabbits) whose red blood cells have little or no aggregability (Table 2) and have not specifically investigated the effect of varying flow rate. Pittman and Ellsworth (32) reported that profiles in arterioles and venules (30–140 μm) of the hamster retractor muscle under both control and reduced flow rates were significantly more blunt [degree of bluntness (B) values (*Eq. 3*) between 0.18 and 0.97] compared with a parabolic profile, possibly due to the averaging effect of the dual-sensor method.

With the use of a high-speed movie camera, Schmid-Schönbein and Zweifach (37) found that velocity profiles in arterioles and venules (16–54 μm) of the rabbit omentum became more blunt (as determined by the ratio of two-dimensional V_{mean} to V_{max}) only at centerline velocities slower than 1.2 mm/s (pseudoshear rate ~20 s^{-1}). Because the aggregability of rabbit blood is less than that of dextran-treated rat blood (Table 2), this result is not surprising.

Velocity profiles in arterioles and venules of the rabbit mesentery using fluorescently labeled platelets as markers (39) were more blunt than those of the present study (K values between 2.3 and 4.0 at higher shear rates) and showed no correlation to the pseudoshear rate over a range of 39–326 s^{-1}. The lack of correlation to shear rate is perhaps due to the small sample size and relatively large scatter of the profile parameters due to interanimal differences. The large blunting parameters reported are unexpected given the low aggregability of rabbit blood but may reflect the smaller diameter of vessels (17–32 μm) in that study.

Methods for characterizing profile shape. Gaehtgens and co-workers (1, 21) devised two dimensionless parameters to quantify the bluntness of velocity profiles. The first of these, R, was defined as the ratio of the volumetric flow rate for the experimentally determined profile versus that for a parabolic profile. The second parameter, F, was defined as the ratio of the area under the experimental profile versus that under a parabolic profile in the region between the tube axis and r/R = 0.5. These two parameters were shown to correlate strongly.

Table 2. *Comparison of erythrocyte aggregability for various species*

Species	ESR, mm/h	Myrenne Aggregometer, M
Hamster		0 ± 0.0*
Rat	0.5 ± 0.2*	0.02 ± 0.1*
Rabbit	1.8 ± 0.6	
Dog	3.5 ± 2.0	
Pig	5.3 ± 2.1	
Cat	5.4 ± 1.3†	5.1 ± 1.3†
Rat (with 0.6% Dextran 500)	8.0 ± 0.5*	11.7 ± 5.5*
Human	10.7 ± 4.0	16 ± 2‡
Horse	71.3 ± 30.0	37 ± 2‡

All values reported as means ± SD. Erythrocyte sedimentation rate (ESR) data from Ref. 2 unless otherwise noted. *Present results. †Results from Ref. 12. ‡Results from Ref. 4.

We determined the parameter F for each of our experimental profiles, as shown in Fig. 12*A*. Whereas the F values in the study of Gaehtgens et al. ranged from 1.1 to 2.9 for human blood with the use of the dual-slit measurement of velocity, the F values in our study ranged between 0.6 and 1.4 for dextran-treated animals, which have a similar aggregation tendency to that of human blood. The statistical power of the regression fits of our experimental data to the parameter F was not as high (i.e., correlation coefficient not as large) as to *Eq. 1* due to loss of a considerable number of data points. However, the same conclusions may be drawn from Fig. 12*A* regarding the characteristics of profiles for both normal and dextran-treated animals as from the previous graphs. The intersection of the regression lines occurs at a value of ~8.7 mm/s, which is not significantly different from the value of 9.2 mm/s shown in Fig. 8.

In our study, the center of the cell image was never closer than ~2.5 μm from the vessel wall. With the use of only those data points between the tube axis and $r/R = 0.5$ in *Eq. 1*, which reduces the number of data points and hence the goodness of the individual regression fits, the relationship shown in Fig. 12*B* is obtained. This relationship is similar to that shown in Figs. 8 and 12*A* and demonstrates that our conclusions are not significantly affected by the ability to obtain velocity points extremely close to the vessel wall.

Pittman and co-workers (19, 31, 32) described the bluntness of velocity profiles in arterioles and venules of the hamster retractor muscle with the use of the equation

$$V(r) = V_{max}\left[1 - B\left(\frac{r^2}{R^2}\right)\right] \quad (3)$$

where the factor B is a parameter describing the degree of bluntness that can vary between 0 for plug flow and 1 for parabolic flow. The relationship between B and V_{max} for our data is shown in Fig. 12*C*. Our profiles with normal blood had B values ranging from 0.9 to 1.1 compared with the hamster profiles, which had B values between 0.18 and 0.97 (19). However, Fig. 12*C* shows that the same conclusions may be drawn about the effective velocity range of red blood cell aggregation with this analysis method as with those described above.

Equation 1 was used previously by Tangelder et al. (39) to describe velocity profiles obtained with fluorescently labeled blood cells in arterioles and venules (17–32 μm) of the rabbit mesentery. It was shown that *Eq. 1* can be modified to describe asymmetrical profiles by inclusion of the parameters a and b

$$V(r) = V_{max}\left[1 - \left|a\left(\frac{r}{R}\right) + b\right|^K\right] \quad (4)$$

where a is a scale factor allowing for a nonzero intercept at the vessel wall and b is a parameter correcting for a shift of V_{max} away from the vessel center. With the use of this equation, Tangelder et al. defined a dimensionless parameter

$$\frac{V_{max}}{V_{mean}} = \frac{(K+2)}{[K+2-2(a)^K]} \quad (5)$$

to characterize their profiles. Applying this method of analysis to each profile in our data, the relationship to V_{max} (actual) is shown in Fig. 12*D*. Again, a significant difference can be detected between the normal and dextran-treated animals, with the intersection of the two regressions occurring at ~9 mm/s.

On review, the four graphs shown in Fig. 12 are qualitatively similar and demonstrate an effect of red

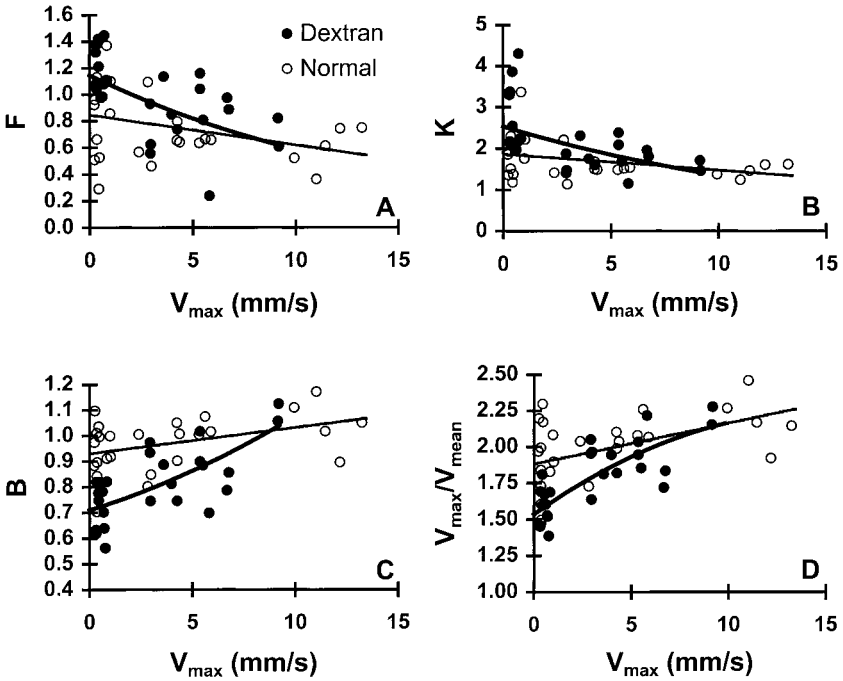

Fig. 12. Comparison of alternative data analysis method parameters versus V_{max} for velocity profiles from normal and dextran-treated rats. Shown are the parameter F from Ref. 21 (*A*), the parameter K from *Eq. 1* using only data values between the tube axis and the radial position (r)/radius of the vessel (R) equal to (B), the parameter B from Refs. 19, 31, and 32 (*C*), and the V_{max}/V_{mean} parameter from Ref. 39 (*D*). $P < 0.05$ for all regression lines.

Table 3. *Summary of profile parameters from various analysis methods*

Vessel Section	D, μm	V_{max} (actual), mm/s	V_{max} (From *Eq. 4*)	a (From *Eq. 4*)	K (From *Eq. 4*)	b (From *Eq. 4*)	V_{max}/V_{mean} (From *Eq. 5*)	F	B (From *Eq. 3*)
					Normal				
1	51.8 ± 7.1	6.0 ± 3.9	0.90 ± 0.07	0.87 ± 0.10	1.31 ± 0.28	−0.01 ± 0.05	2.07 ± 0.08	0.66 ± 0.10	0.99 ± 0.06
2	57.6 ± 10.0	7.2 ± 4.3	0.90 ± 0.06	0.90 ± 0.08	1.34 ± 0.13	0.01 ± 0.06	2.10 ± 0.22	0.74 ± 0.22	1.02 ± 0.12
3	55.5 ± 9.1	7.2 ± 4.1	0.91 ± 0.06	0.84 ± 0.12	1.19 ± 0.26	−0.003 ± 0.06	2.09 ± 0.21	0.57 ± 0.15	0.99 ± 0.13
1	47.9 ± 4.7	0.49 ± 0.33	0.87 ± 0.05	0.92 ± 0.07	1.73 ± 0.33	−0.05 ± 0.04	1.94 ± 0.32	0.88 ± 0.17	0.95 ± 0.17
2	54.9 ± 8.9	0.51 ± 0.34	0.90 ± 0.03	0.91 ± 0.11	1.65 ± 0.61	−0.01 ± 0.08	2.00 ± 0.21	0.76 ± 0.42	0.96 ± 0.06
3	53.4 ± 8.0	0.47 ± 0.26	0.91 ± 0.04	0.89 ± 0.11	1.77 ± 0.65	0.02 ± 0.02	1.88 ± 0.20	0.97 ± 0.35	0.97 ± 0.07
					Dextran				
1	53.1 ± 4.2	4.5 ± 1.4	0.96 ± 0.07	0.74 ± 0.11	1.06 ± 0.40	−0.04 ± 0.06	1.98 ± 0.19	0.69 ± 0.38	0.85 ± 0.10
2	55.0 ± 10.5	5.6 ± 2.5	0.89 ± 0.08	0.87 ± 0.11	1.40 ± 0.38	−0.01 ± 0.06	2.01 ± 0.17	0.86 ± 0.16	0.96 ± 0.13
3	52.6 ± 10.6	5.7 ± 2.4	0.93 ± 0.05	0.80 ± 0.12	1.33 ± 0.28	−0.004 ± 0.03	1.86 ± 0.20	0.86 ± 0.21	0.85 ± 0.13
1	48.5 ± 4.3	0.51 ± 0.24	0.80 ± 0.12	0.82 ± 0.03	1.75 ± 0.27	−0.04 ± 0.07	1.63 ± 0.12	1.05 ± 0.06	0.77 ± 0.10
2	51.9 ± 7.4	0.54 ± 0.20	0.78 ± 0.12	0.83 ± 0.08	2.14 ± 0.51	0.02 ± 0.03	1.52 ± 0.11	1.17 ± 0.16	0.68 ± 0.10
3	54.2 ± 10.4	0.53 ± 0.20	0.78 ± 0.10	0.91 ± 0.15	2.73 ± 0.87	0.01 ± 0.06	1.58 ± 0.16	1.32 ± 0.17	0.69 ± 0.07

All values reported as means ± SD. a, Scale factor for nonzero intercept; b, parameter correcting for shift; F, ratio of the area under the experimental profile vs. that under a parabolic profile in the region between the tube axis and the radial position divided by the radius of the vessel equals 0.5; B, degree of bluntness.

blood cell aggregation on velocity profiles independent of the particular method used. The profile parameters for these alternate methods are summarized in Table 3. A complete listing of the parameters for each individual profile is on file in the journal repository as Table B.[2]

Asymmetry of velocity profiles. In vitro velocity profiles determined in tubes where length is several orders of magnitude greater than diameter are usually axisymmetric (1, 10, 21). However, venular network geometry is characterized by frequent bifurcations, which combine blood streams that may be of different velocities and hematocrit into the same flow stream. It has been shown in theoretical studies by Popel and co-workers (17, 18) that asymmetric velocity profiles may result when streams of different hematocrit converge. The degree of asymmetry in velocity profiles can be expressed in a quantitative form using parameter b from *Eq. 4*. In our profiles, the parameter b had an average value of -0.008 ± 0.053, which is not significantly different from zero ($P > 0.05$), and is equivalent to shifting the center of the profile 0.13 μm toward the wall in a 50-μm vessel. The asymmetry indexes are not significantly different for profiles from sections upstream or downstream from bifurcations ($P > 0.05$) for both dextran-treated and normal blood ($P > 0.05$). It is possible that by averaging cell velocities over a 100-μm section length, asymmetry at localized sites is also averaged. In the studies of Tangelder et al. (39), the b value was also not significantly different from zero at a measurement site six vessel diameters downstream from a bifurcation. In those studies, profiles were obtained from a large number of velocity readings at each radial position over a longitudinal distance of 35–45 μm, effectively averaging out the random fluctuations as in our study. On the basis of the theoretical models, it would appear that the converging streams studied in the present experiments were of similar hematocrit.

Schmid-Schönbein and Zweifach (37) reported velocity profiles in arterioles and venules of the rabbit omentum that were markedly asymmetric. However, examination of their profiles does not reveal a repeatable pattern. Velocity profiles obtained at several locations in an unbranched vessel had significantly different shapes even though no intervening bifurcations were present. Similarly, Ellsworth and Pittman (19) found that, in hamster retractor muscle arterioles and venules (30–140 μm), 41% of the profiles were significantly asymmetric. Because in both of these studies the velocity was determined at 5–11 radial positions, it is possible that a larger number of measurements would have yielded more symmetric profiles. However, it is also possible that nonuniform hematocrit distribution was responsible for the asymmetry.

Effect of shear rate on red blood cell aggregation in vivo. Our study shows that venular velocity profiles are significantly affected by red blood cell aggregation at pseudoshear rates (V_{mean}/diameter) up to 40 s^{-1} (Fig. 8). The qualitative similarity of the present results to previous rotational viscometric data (13, 14) suggests that the exponent K is a suitable index that can be used to describe the effect of aggregation on blood flow in vivo. The rotational viscometric studies show that red blood cell aggregation increases the apparent viscosity of human blood at shear rates below 5 s^{-1}. With the use of this value as a benchmark for determining whether or not aggregates might be present at a given radial position at the lowest flow rates studied, it can be seen that aggregation extends this region by 15% of the radius on average (Fig. 11*A*) and up to 45% in the most extreme case. At faster flow rates, the center of the vessel may contain red blood cell aggregates even when the pseudoshear rate is so high that aggregate formation would not occur if the shear rate had remained a linear function of radial position.

[2]For Table B (Comparisons of Profile Parameters from Various Analysis Methods), order NAPS Document 05581 from NAPS % Microfiche Publications, PO Box 3513, Grand Central Station, New York, NY 10017.

Implications of profile blunting for vascular resistance. Previous studies in the dog intestine (26), dog hindlimb (41), cat sartorius muscle (25), and cat lateral gastrocnemius muscle (12) preparations have reported increases in venous vascular resistance of up to 300% on reduction of arterial pressure from 100 to 40 mmHg. In a cat muscle preparation (12), it was shown that most, if not all, of this increase could be explained by the presence of red blood cell aggregation. Previous studies also showed that nearly 70% of the pressure drop in the venous network of cat sartorius muscle occurs across the venules in the diameter range of 25–185 μm (25) and that the diameter of these vessels changes very little during large changes in arterial pressure (24). The latter finding has been confirmed by us (8) in rat spinotrapezius muscle for both horizontally and vertically oriented venules. The pseudoshear rate in venules of cat sartorius muscle (24) at normal arterial pressure approaches the range ($<10\ s^{-1}$) where red blood cell aggregation has been shown to increase blood viscosity in vitro (9, 13, 14, 30, 34).

To estimate the possible effect of a blunted velocity profile on venous vascular resistance, the shear stress at the vessel wall (τ_W) was determined by differentiation of *Eq. 1*, yielding the equation

$$\tau_W = \frac{\mu_{blood} \cdot V_{max} \cdot K}{R} \qquad (6)$$

where μ_{blood} is the blood viscosity, V_{max} and K are the profile parameters from *Eq. 1*, and R is the vessel radius. From *Eq. 6*, it can be seen that the shear stress at the venular wall with a blunted velocity profile is greater than that for Poiseuille flow with the same V_{max} by a factor of $K/2$. As shown in Figs. 8 and 10, the parameter K for the profiles obtained with dextran-treated blood reaches a value near 4.0 (3.2 ± 0.3, range 2.3–4.3) in a number of instances at the lowest shear rates. Assuming the viscosity of the blood near the wall is similar at high and low flows, this relationship is directly analogous to that shown in Fig. 11 and would correspond to an increase in vascular resistance of ~100% over control levels at these lowest shear rates.

Two factors might influence the viscosity of the blood near the wall: red blood cell deformation and red blood cell axial migration. On the basis of rotational viscometric studies of human blood (13, 14), red blood cell deformation is estimated to decrease the viscosity of blood near the wall by ~5% at V_{max} = 0.2 mm/s (Fig. 11*A*) and ~3% at V_{max} = 4.0 mm/s (Fig. 11*B*). However, because red blood cell aggregation increases resistance and reduces flow velocity at the same driving pressure, the actual effect would be even less. Studies in glass tubes (1, 16, 34) have shown an increased tendency for red blood cell axial migration to occur on aggregate formation, leading to a decreased fluid viscosity near the wall of the tube. In a steady-state flow situation, this decreased viscosity near the wall may be large enough to effectively cancel out the increase in vascular resistance caused by an increased viscosity in the red blood cell core area due to red blood cell aggregation (34). However, red blood cell axial migration is a time-dependent process that requires 30–300 s to reach a steady-state value (1). In glass tube studies where the tube length is several orders of magnitude larger than the diameter, such a process would occur to a much larger degree than in vivo, where frequent bifurcations in the venous network cause a constant infusion of red blood cells and aggregates into the peripheral layer of the flow stream. In addition, red blood cell aggregation increases the margination and adherence of leukocytes in venules (20), which would further increase venous vascular resistance beyond that due to blunted velocity profiles alone; leukocyte-endothelium adhesion significantly increases vascular resistance (29).

Whereas the aggregation tendency of the dextran-treated blood in our study is somewhat higher than both cat and dog blood as shown in Table 2, our data on velocity profiles may be applicable to the venous vascular beds of those species and the changes in venous resistance. Our findings agree with the conclusion of Das et al. (18), on the basis of a theoretical analysis, that changes in shear stress distribution due to blunted velocity profiles could cause significant flow-dependent changes in resistance in the venular circulation of the cat. As also shown in Table 2, the aggregability of human blood is greater and that of the horse is much greater than the dextran-treated rat blood, which may have implications for flow-dependent changes in venous resistance in those species.

Extent of red blood cell aggregation in circulation. It has long been considered that for those species (such as cats, dogs, and humans) in which it is a naturally occurring phenomenon, red blood cell aggregation may have a significant effect on vascular resistance in segments of the circulation other than the venular network, but these considerations have been limited to circulatory shock and other low flow states (12, 28). Our data provide a quantitative basis for evaluating this suggestion. On the basis of average values for flow and diameter, pseudoshear rates in humans have been estimated to be less than 40 s^{-1} in most segments of the arterial network and in all segments of the venous network at normal flow rates (45). Therefore, it is likely that red blood cell aggregation is normally present to some degree in most areas of the circulation (excluding the capillaries and other small vessels). In support of this possibility, a number of investigators have reported an ultrasonic backscattering effect of red blood cell aggregates in the large arteries and veins (15). Those observations, coupled with the present results, raise the possibility that red blood cell aggregation may have significant effects on effective blood viscosity in other segments of the circulation. Such effects would be more prominent in low flow states, such as shock, where cardiac output may fall to 25% of normal values and shear rate in individual vessels may also fall to a similar extent (27), depending on local changes in vascular diameter. Our data suggest that the effect of

aggregation on vascular resistance outside the venular network would be significant, but its magnitude cannot be estimated from the data presently available.

The authors thank Dr. Amy Tsai for many valuable discussions and for providing samples of hamster blood for ESR and aggregation measurements. We also thank Dr. Heng-Chuan Kan for helpful discussions and Masoud Paknejad, Caroline Flarity, Andilily Lai, Nhat Nguyen, and Rami Apelian for technical assistance in data acquisition.

This work was supported by National Heart, Lung, and Blood Institute Grant HL-52684.

REFERENCES

1. **Alonso C, Pries AR, Kiesslich O, Lerche D, and Gaehtgens P.** Transient rheological behavior of blood in low-shear tube flow: velocity profiles and effective viscosity. *Am J Physiol Heart Circ Physiol* 268: H25–H32, 1995.
2. **Altman P.** *Blood and Other Body Fluids*, edited by Ditmer D. Washington, DC: FASEB, 1961.
3. **Baker M and Wayland H.** On-line volume flow rate and velocity profile measurement for blood in microvessels. *Microvasc Res* 7: 131–143, 1974.
4. **Baskurt OK, Farley RA, and Meiselman HJ.** Erythrocyte aggregation tendency and cellular properties in horse, human, and rat: a comparative study. *Am J Physiol Heart Circ Physiol* 273: H2604–H2612, 1997.
5. **Baskurt OK, Meiselman HJ, and Kayar E.** Measurement of red blood cell aggregation in a "plate-plate" shearing system by analysis of light transmission. *Clin Hemorheol Microcirc* 19: 307–314, 1998.
6. **Bishop J, Nance P, Flarity C, Paknejad M, Lai A, Popel A, Intaglietta M, and Johnson PC.** Skeletal muscle venule velocity profiles with labeled cell and dual window techniques (Abstract). *FASEB J* 13: A425, 1999.
7. **Bishop J, Nance P, Popel A, Intaglietta M, and Johnson PC.** Red blood cell aggregation in the venous network (Abstract). *J Vasc Res* 35*, Suppl* 2: P167, 1998.
8. **Bishop JJ, Nance P, Popel AS, Intaglietta M, and Johnson PC.** Diameter changes in skeletal muscle venules during arterial pressure reduction. *Am J Physiol Heart Circ Physiol* 279: H47–H57, 2000.
9. **Brooks DE, Goodwin JW, and Seaman GVF.** Interactions among erythrocytes under shear. *J Appl Physiol* 28: 172–177, 1970.
10. **Bugliarello G and Hayden JW.** Detailed characteristics of the flow of blood in vitro. *Trans Soc Rheol* 7: 209–230, 1963.
11. **Bugliarello G and Sevilla J.** Velocity distribution and other characteristics of steady and pulsatile blood flow in fine glass tubes. *Biorheology* 7: 85–107, 1970.
12. **Cabel M, Meiselman HJ, Popel AS, and Johnson PC.** Contribution of red blood cell aggregation to venous vascular resistance in skeletal muscle. *Am J Physiol Heart Circ Physiol* 272: H1020–H1032, 1997.
13. **Chien S.** Shear dependence of effective cell volume as a determinant of blood viscosity. *Science* 168: 977–978, 1970.
14. **Chien S, Usami S, Dellenback RJ, and Gregersen MI.** Shear-dependent interaction of plasma proteins with erythrocytes in blood rheology. *Am J Physiol* 219: 143–153, 1970.
15. **Cloutier G and Qin Z.** Ultrasound backscattering from non-aggregating and aggregating erythrocytes–a review. *Biorheology* 34: 443–470, 1997.
16. **Cokelet GR and Goldsmith HL.** Decreased hydrodynamic resistance in the two-phase flow of blood through small vertical tubes at low flow rates. *Circ Res* 68: 1–17, 1991.
17. **Das B, Enden G, and Popel AS.** Stratified multiphase model for blood flow in a venular bifurcation. *Ann Biomed Eng* 25: 135–153, 1997.
18. **Das B, Johnson PC, and Popel AS.** Effect of nonaxisymmetric hematocrit distribution on non-Newtonian blood flow in small tubes. *Biorheology* 35: 69–87, 1998.
19. **Ellsworth ML and Pittman RN.** Evaluation of photometric methods for quantifying convective mass transport in microvessels. *Am J Physiol Heart Circ Physiol* 251: H869–H879, 1986.
20. **Fahraeus R.** The influence of the rouleau formation of the erythrocytes on the rheology of the blood. *Acta Med Scand* 161: 151–165, 1958.
21. **Gaehtgens P, Meiselman HJ, and Wayland H.** Velocity profiles of human blood at normal and reduced hematocrit in glass tubes up to 130 μ diameter. *Microvasc Res* 2: 13–23, 1970.
22. **Glantz SA.** *Primer of Biostatistics*. San Franscisco, CA: McGraw-Hill, 1997.
23. **Gretz JE and Duling BR.** Measurement uncertainties associated with the use of bright-field and fluorescence microscopy in the microcirculation. *Microvasc Res* 49: 134–140, 1995.
24. **House SD and Johnson PC.** Diameter and blood flow of skeletal muscle venules during local flow regulation. *Am J Physiol Heart Circ Physiol* 250: H828–H837, 1986.
25. **House SD and Johnson PC.** Microvascular pressure in venules of skeletal muscle during arterial pressure reduction. *Am J Physiol Heart Circ Physiol* 250: H838–H845, 1986.
26. **Johnson PC and Hanson KM.** Effect of arterial pressure on arterial and venous resistance of intestine. *J Appl Physiol* 17: 503–508, 1962.
27. **Kerger H, Waschke KF, Ackern KV, Tsai AG, and Intaglietta M.** Systemic and microcirculatory effects of autologous whole blood resuscitation in severe hemorrhagic shock. *Am J Physiol Heart Circ Physiol* 276: H2035–H2043, 1999.
28. **Knisely MH.** Intravascular erythrocyte aggregation (blood sludge). In: *Handbook of Physiology*, *Circulation*. Bethesda, MD: Am. Physiol. Soc., 1965, sect. 2, vol. III, chapt. 63, p. 2249–2292.
29. **Lipowsky HH, Usami S, and Chien S.** In vivo measurements of "apparent viscosity" and microvessel hematocrit in the mesentery of the cat. *Microvasc Res* 19: 297–319, 1980.
30. **Merrill EW, Gilliland ER, Cokelet G, Shin H, Britten A, and Wells RW.** Rheology of blood and flow in the microcirculation. *J Appl Physiol* 18: 255–260, 1963.
31. **Parthasarathi AA, Japee SA, and Pittman RN.** Determination of red blood cell velocity by video shuttering and image analysis. *Ann Biomed Eng* 27: 313–325, 1999.
32. **Pittman RN and Ellsworth ML.** Estimation of red blood cell flow in microvessels: consequences of the Baker-Wayland spatial averaging model. *Microvasc Res* 32: 371–388, 1986.
33. **Popel AS, Johnson PC, Kameneva MV, and Wild MA.** Capacity for red blood cell aggregation is higher in athletic mammalian species than in sedentary species. *J Appl Physiol* 77: 1790–1794, 1994.
34. **Reinke W, Gaehtgens P, and Johnson PC.** Blood viscosity in small tubes: effect of shear rate, aggregation, and sedimentation. *Am J Physiol Heart Circ Physiol* 253: H540–H547, 1987.
35. **Reinke W, Johnson PC, and Gaehtgens P.** Effect of shear rate variation on apparent viscosity of human blood in tubes of 29 to 94 μm diameter. *Circ Res* 59: 124–132, 1986.
36. **Rosenblum WI.** Ratio of red blood cell velocities near the vessel wall to velocities at the vessel center in cerebral microcirculation, and an apparent effect of blood viscosity on this ratio. *Microvasc Res* 4: 98–101, 1972.
37. **Schmid-Schönbein GW and Zweifach BW.** RBC velocity profiles in arterioles and venules of the rabbit omentum. *Microvasc Res* 10: 153–164, 1975.
38. **Shonat RD and Johnson PC.** Oxygen tension gradients and heterogeneity in venous microcirculation: a phosphorescence quenching study. *Am J Physiol Heart Circ Physiol* 272: H2233–H2240, 1997.
39. **Tangelder GJ, Slaaf DW, Muijtjens AMM, Arts T, oude Egbrink MGA, and Reneman RS.** Velocity profiles of blood platelets and red blood cells flowing in arterioles of the rabbit mesentery. *Circ Res* 59: 505–514, 1986.
40. **Tangelder GJ, Slaaf DW, Teirlinck HC, Alewijnse R, and Reneman RS.** Localization within a thin optical section of

fluorescent blood platelets flowing in a microvessel. *Microvasc Res* 23: 214–230, 1982.
41. **Thulesius O and Johnson PC.** Pre- and postcapillary resistance in skeletal muscle. *Am J Physiol* 210: 869–872, 1966.
42. **Unthank JL, Lash JM, Nixon JC, Snider RA, and Bohlen HG.** Evaluation of carbocyanine-labeled erythrocytes for microvascular measurements. *Microvasc Res* 45: 193–210, 1993.
43. **Usami S, Chien S, and Gregersen MI.** Viscometric characteristics of blood of the elephant, man, dog, sheep, and goat. *Am J Physiol* 217: 884–890, 1969.
44. **Wayland H and Johnson PC.** Erythrocyte velocity measurement in microvessels by a two-slit photometric method. *J Appl Physiol* 22: 333–337, 1967.
45. **Whitmore RL.** *Rheology of the Circulation*. New York: Pergamon, 1968.